Effect of geometric parameters on performance of supersonic ejector

N.I. Hewedy, Mofreh H. Hamed, F. Sh. Abou-Taleb and Tarek A. Ghonim

Mechanical Power Eng. Dept., Faculty of Eng., Menoufiya University, Shebin El-Kom, Egypt
e-mail: mofrehh@ yahoo.com

This paper describes and evaluates a new theoretical method for designing supersonic ejectors. The method predicts numerically the optimum geometry of an ejector which gives maximum efficiency. The numerical investigation is based on flow equations governing turbulent, compressible, two-dimensional, steady, time averaged and boundary layer equations. These equations are continuity, momentum and energy. In addition, turbulent shear stress and heat transfer are calculated using eddy viscosity model. These equations are solved iteratively using finite difference method under the conditions of different flow regimes which can be divided into several distinctive regions where, the methods for estimating the mixing length are different for each flow region. The first flow region depicts the wall boundary layer, jet shear layer and secondary and primary potential flow. The second one contains a single region of developing flow. Simple ejectors with convergent-divergent primary nozzle were fabricated and tested experimentally to evaluate the proposed method. The present theoretical and experimental results are well compared with the published data. The results obtained are used to correlate the optimum ejector geometry, pressure ratio and ejector optimum efficiency as functions of the operation parameters and ejector area ratio. The resultant correlations help in selecting the optimum ejector geometry and its corresponding maximum efficiency for particular operating conditions.

تهتم هذه الورقة بدراسة معملية وعددية لحساب الأبعاد المثلى لحاقن نافوري والتى تعطي كفاءة أداء قصوى. تعتمد الدراسة العددية على المعادلات الخاصة بالسريان الأضطرابي الأنضغاطي ثنائي الأبعاد المستقر وهي معادلات الاستمرارية وبقاء كمية التحرك وبقاء الطاقة ومعادلات الطبقة المتاخمة. كما تم استخدام نموذج "eddy" في حساب انتقال الحرارة والاحتكاك الاضطرابي. تم حل المعادلات السابقة بطريقة تكرارية باستخدام طريقة الفروق المحددة الضمنية. وللدراسة المعملية تم تصنيع نموذج لحاقن نافوري متغير المقطع واختباره عمليا. ولاختبار النموذج المقترح تم عقد مقارنة بين نتائج البحث النظرية والمعملية الحالية والمعملية والنظرية المنشورة لآخرين. وقد أظهرت هذه المقارنة توافقا مقبولا. تم استخدام النتائج النظرية في استنتاج علاقات تربط كل من أبعاد الحاقن المثلى، نسبة الانضغاط، كفاءة الحاقن القصوى كدالة في متغيرات التشغيل ونسبة المساحة للحاقن وتحديد مدى استخدام هذه المعادلات المستنتجة فى اختيار أبعاد الحاقن المثلى المقابلة لأقصى كفاءة للتشغيل عند ظروف تشغيل مختلفة. وللتحقق من هذه العلاقات المستنتجة تم اختبار ثلاث أبعاد مثلى مختلفة لحاقن نافورى تم حسابها من العلاقات المستنتجة وإختبارها معمليا ومقارنتها بنتائج العلاقات المستنتجة. وقد أظهرت هذه المقارنة توافقا مقبولاً.

Keywords: Optimum ejector geometry, Supersonic flow, Two-dimensional flow, Ejector area ratio, Maximum ejector efficiency

1. Introduction

For many years, ejectors utilizing readily available fluids have been employed in industry to economically produce vacuums and pump secondary fluids. Fig. 1 presents a view of typical ejector and its principal components. As shown, two streams of differing momentum are injected into a duct where the higher momentum stream (primary fluid) sucks the lower momentum (secondary fluid) via entrainment. Ejector efficiency and its performance are based on the ability of the adjacent streams to adequately mix and exchange momentum. Many studies [1-11] were directed toward understanding of the flow phenomena and performance of ejectors. Donald and Robert [1] carried out an experimental and theoretical investigation at supersonic and subsonic Mach numbers of auxiliary inlets supplying secondary air flow to ejectors exhaust nozzle. The tests were extensively conducted on two ejector configurations over a wide range of primary nozzle pressure-ratios at Mach numbers of 0.64, 1.5, 1.8 and 2.0. Fabri and Paulon [2] studied experimentally and theoretically supersonic air-air ejectors. The theoretical
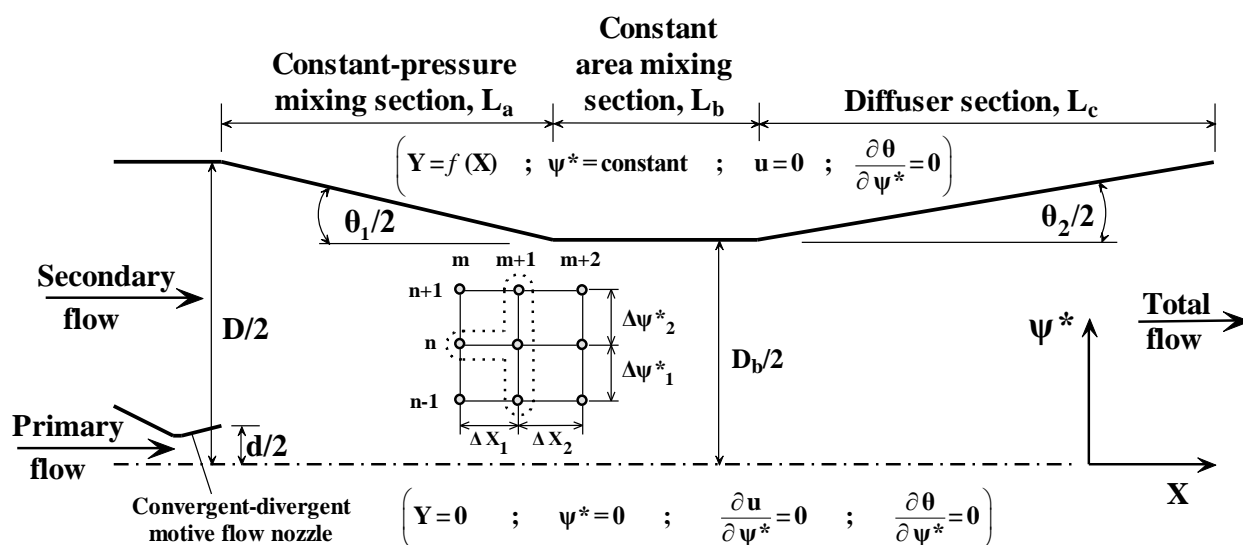
Fig.1. Ejector geometry, boundary conditions and computational grid.

analysis was based on one-dimensional flow and experimental study was conducted on a constant-area mixing ejector. The effects of different parameters such as length of the mixer, terminating diffuser length, cross section of the mixer and primary flow Mach number were studied theoretically. Kirti et al. [3] studied numerically the turbulent mixing in the initial region of heterogeneous axisymmetric coaxial confined jets. A binary isothermal system of non-reacting gases was considered. Their results were obtained for four different jet configurations for which experimental data were available. A formulation was presented for the eddy viscosity and the eddy diffusivity that adequately describes the confined turbulent mixing of heterogeneous streams in the initial region. Abou-Taleb [4] studied experimentally and analytically the effect of geometric parameters on the performance of ejectors. Approximate formulas for calculating pressure ratio and optimum entrainment ratio as well as the optimum design conditions were derived. Dutton and Carroll [5] developed a one-dimensional constant area flow model for solving a large class of supersonic ejector optimization problems. Design curves for common case of adiabatic primary and secondary gases of equal molecular weight and stagnation temperature were also presented in their

study and discussed. Raman and Taghavi [6] provided a detailed experimental evaluation of a rectangular, multi-element, supersonic jet mixer-ejector nozzle. Information on the mixing, pumping, ejector wall pressure distribution characteristics of four simple, multi-element, jet mixer-ejector configurations was presented. Their results showed that the ejector configuration that produced the maximum entrainment ratio also exhibited the lowest wall pressures in the inlet region and maximum thrust augmentation. Guillaume and Judge [7] presented a unique means of increasing the efficiency of a jet pump by using elliptical nozzles on jets instead of round jets. At high flow rates, the jet pump using the elliptical jets was shown to have an efficiency that was approximately a factor of 6 greater than the pump using the round jets. Szabo [8] studied analytically the influence of the material quality of the primary gas jets on the final vacuum created by a supersonic gas ejector. His results showed that their ejector geometry greatly depended on the quality changes of the operating primary gas due to temperature and pressure changes. Kandakure et al. [9] developed a numerical model to understand the hydrodynamic characteristics with reference to ejector geometry and the effects of operating conditions on the ejector performance.

Karambirov and Chebaevskii [10] described a method of choosing an ejector geometry for given operating conditions. Generalized dimensionless characteristics of ejectors were given for averaged loss coefficients. They explored the possibility of decreasing the coefficients of heat loss by improving the profile for the delivery of passive fluids to an ejector pump (use of stepped diffuser). Yong et al. [11] studied numerically and experimentally the development of a large-entrainment-ratio axisymmetric supersonic ejector for micro butane combustor. Operation conditions as well as geometric parameters of the ejector were systematically changed and their effects on the volume-flow-rate ratio were investigated in a series of experiments where butane was mostly simulated by air. Most of previous publications did not concern with overall efficiency enhancement by optimization of the geometric parameters and choosing of the operating conditions in order to give the maximum overall ejector efficiency, which is the primary motivation behind the present work.

2. Experimental set-up

The experimental set-up is schematized in fig. 2. Compressor of sufficient capacity is used to ensure the continuous operation of the ejector. Compressed air (at a maximum pressure of about 8 bars and an ambient stagnation temperature) is filtered to remove large particles such as dust and compressed oil droplets. The compressed air is then directed towards an air reservoir which is connected to the entrance of the primary flow nozzle of the ejector. A pressure control valve is used to adjust the primary flow stagnation pressure P_{o1}. The entrained air flow is taken from the surrounding atmosphere. The entrained mass flow rate can be regulated by means of a valve located at the entrance of the aspiration tube.

Apparatuses installed on the primary and secondary air circuits to measure the stagnation pressures and mass flow rates are also shown in fig. 2. Pressure taps distributed along the ejector were used to measure wall static pressure distributions.

In the tested ejector as illustrated in fig. 1, the exit diameter of the primary flow nozzle is 6.2 mm (inner), the dimensionless constant pressure mixing section length (L_a/D_b), constant area mixing section length (L_b/D_b), diffuser section length (L_c/D_b) and area ratio (Ar) are 4.08, 4.46, 8.9 and 17.38 respectively while the total angles of the constant pressure mixing section and the diffuser section, θ_1 and θ_2, are 5.4° and 2.7° respectively. The uncertainty for all the measuring devices was found to be in the range of 0.08% to 5.6 %.

3. Mathematical model

The flow through the ejector is modeled based on the governing flow equations under the following assumptions:
- Two-dimensional and steady flow.
- Both stream flows are the same perfect gas.
- No heat transfer across the walls of the ejector.
- Both streams are assumed to be skockless.
- Static pressure is constant at any section normal to the axial direction.

3.1. Governing equations

The system of equations governing turbulent, compressible, steady, time-averaged and boundary layer flow can be written as follows:

- *Continuity equation*

$$\frac{\partial \bar{\rho}\,\bar{u}}{\partial x} + \frac{1}{r}\frac{\partial\left(\bar{\rho}\,\bar{v}\,r\right)}{\partial r} = 0\,. \tag{1}$$

- *Momentum equation*

$$\bar{\rho}\,\bar{u}\frac{\partial \bar{u}}{\partial x} + \bar{\rho}\,\bar{v}\frac{\partial \bar{u}}{\partial y} =$$
$$-\frac{d\,\bar{p}}{d\,x} + \frac{1}{y^{\alpha}}\frac{\partial}{\partial y}\left[\bar{\mu}\,y^{\alpha}\frac{\partial \bar{u}}{\partial y} - y^{\alpha}\overline{u'\,(\rho v)'}\right]. \tag{2}$$
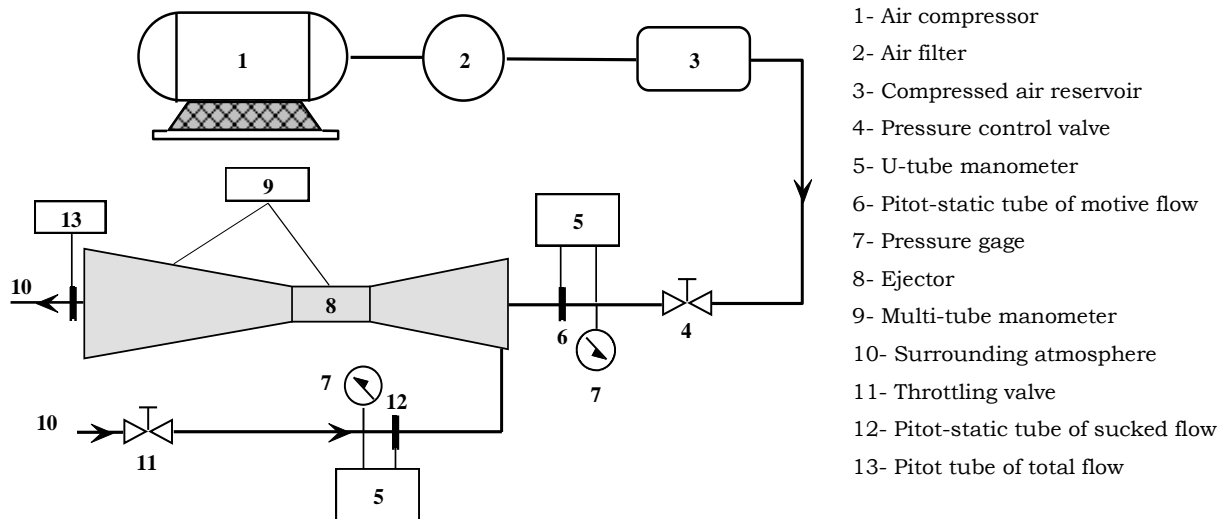
Fig. 2. Experimental setup.

1- Air compressor
2- Air filter
3- Compressed air reservoir
4- Pressure control valve
5- U-tube manometer
6- Pitot-static tube of motive flow
7- Pressure gage
8- Ejector
9- Multi-tube manometer
10- Surrounding atmosphere
11- Throttling valve
12- Pitot-static tube of sucked flow
13- Pitot tube of total flow

- *Energy equation*

$$\bar{\rho}\,\bar{u}\,\bar{c}_p\,\frac{\partial \bar{T}}{\partial x} + \bar{\rho}\,\bar{v}\,\bar{c}_p\,\frac{\partial \bar{T}}{\partial y} = \bar{u}\,\frac{\partial \bar{p}}{\partial x} + \frac{1}{y^\alpha}\frac{\partial}{\partial y}$$
$$\left[\bar{k}\,y^\alpha\frac{\partial \bar{T}}{\partial y} - \bar{c}_p\,y^\alpha\overline{(\rho v)'\,T'}\right]$$
$$+\bar{\mu}\left(\frac{\partial \bar{u}}{\partial y}\right)^2 - \overline{u'(\rho v)'}\,\frac{\partial \bar{u}}{\partial y}$$
(3)

Where $\alpha = 1$, $y = r$ for axisymmetric flow and $\alpha = 0$ for two-dimensional flow.

For axisymmetric flow, the above system of equations can be rewritten in terms of stream function, ψ using the proposed transformation by Krause [12 and 15] as follows:

$$\bar{u}\,\frac{\partial \bar{u}}{\partial x} = -\frac{1}{\bar{\rho}}\frac{d \bar{p}}{d x} + \frac{\bar{u}}{2\psi}\frac{\partial}{\partial \psi}$$
$$\left[\frac{\bar{u}\,\bar{\rho}\,\bar{u}\,r^2}{2\psi}\frac{\partial}{\partial \psi} - \overline{u'(\rho v)'}\,r\right].$$
(4)

$$\bar{u}\,\bar{c}_p\,\frac{\partial \bar{T}}{\partial x} = \frac{\bar{u}}{\bar{\rho}}\frac{d \bar{p}}{d x} + \frac{\bar{u}}{2\psi}\frac{\partial}{\partial \psi}$$
$$\left[\frac{\bar{k}\,\bar{\rho}\,\bar{u}\,r^2}{2\psi}\frac{\partial \bar{T}}{\partial \psi} - \bar{c}_p\,\overline{T'(\rho v)'}\,r\right] + \frac{\Phi}{\bar{\rho}}.$$
(5)

Where,

$$\Phi = \left(\frac{\bar{\rho}\,\bar{u}\,r}{2\psi}\frac{\partial \bar{u}}{\partial \psi}\right)^2 - \overline{u'(\rho v)'}\left(\frac{\bar{\rho}\,\bar{u}\,r}{2\psi}\frac{\partial \bar{u}}{\partial \psi}\right)$$

$$\frac{\partial \psi^2}{\partial y} = \bar{\rho}\,\bar{u}\,r\,; \qquad \frac{\partial \psi^2}{\partial x} = \bar{\rho}\,\bar{v}\,r.$$

Using the eddy viscosity model, the "turbulent shear stress" and "turbulent heat transfer" are defined by:

$$\tau_T = \bar{\rho}\,\varepsilon\,\frac{\partial \bar{u}}{\partial r} = -\overline{u'(\rho v)'} = \frac{\bar{\rho}^2\bar{u}\,r\,\varepsilon}{2\psi}\frac{\partial \bar{u}}{\partial \psi},$$
(6)

$$q_T = \bar{\rho}\,\bar{c}_p\varepsilon_H\,\frac{\partial \bar{T}}{\partial r} = -\overline{c_p(\rho v)'\,T'} = \frac{\bar{\rho}^2\bar{u}\,r}{2\psi}\,\bar{c}_p\,\varepsilon_H\,\frac{\partial \bar{T}}{\partial \psi}.$$
(7)

Where ε is termed the "eddy momentum diffusivity" and ε_H is the "eddy thermal diffusivity".

After substitution from eqs. (6 and 7), eqs. (4 and 5) can be expressed in a dimensionless form and regrouping in X - ψ^* coordinates [15] as;

$$u\,\frac{\partial u}{\partial X} = -\frac{1}{2\rho^*}\frac{d p}{d X} + \frac{u}{2\psi^*}\frac{\partial}{\partial \psi^*}\left[S\,\frac{\partial u}{\partial \psi^*}\right].$$
(8)

$$u \; c_p{}^* \; \frac{\partial \theta}{\partial X} = \frac{C_L}{2\rho^*} u \frac{d\,p}{dX} + \frac{C_L S}{2\psi^*} \left(\frac{\partial u}{\partial \psi^*} \right)^2$$
$$- \frac{u}{2\psi^*} \; \frac{\partial}{\partial \psi^*} \left(Q \frac{\partial \theta}{\partial \psi^*} \right). \qquad (9)$$

Where:

$$C_L = \frac{(\gamma - 1) M_1{}^2}{\dfrac{T_{wr}}{T_1} - 1}.$$

$$Q = \left(\frac{\mu^*}{P_{r1}} + \frac{E\,\rho^*}{P_{rt}} \right) \frac{Y^2 \rho^* u}{2\,\psi^*}.$$

$$S = \left(\frac{\mu^* + E\,\rho^*}{2\,\psi^*} \right) Y^2 \rho^* u.$$

3.2. Turbulent shear stress and heat transfer

The well-known Prandtl assumption for the turbulent shear stress and heat transfer is:

$$\varepsilon = l_m{}^2 \frac{\partial \bar{u}}{\partial r} . \qquad (10)$$

In a dimensionless form and X - ψ^* coordinates, eq. (10) becomes:

$$E = \frac{u\,\rho^* Y}{2\,\psi^*} L_m{}^2 \left| \frac{\partial u}{\partial \psi^*} \right|$$

For specifying the approximate relationship between the mixing length and the mean flow variables, confined jet mixing, as reported in [13], can be split into several distinctive regions as shown in fig. 3. The first region is called regime-1, which contains the wall boundary layer, jet shear layer, secondary and primary potential flow regions. While the second one is called regime-2 which contains a single region of developing flow. The methods of estimating mixing length are different in each flow region. In the jet shear layer, the mixing length is assumed to be dependent only on the shear layer width. The definitions of the wall boundary layer thickness and shear layer thickness were based on the value of r at which the local velocity was 0.99 of the external stream velocity and taken as depicted in [15].

3.3. Finite difference equations

The general form of differential eqs. (8 and 9) in finite-differencing form according to grid lines shown in fig. 1 is:

$$A_{n\text{-}1}\,\beta_{m+1,n} + B_{n\text{-}1}\,\beta_{m+1,n+1} + C_{n\text{-}1}\,\beta_{m+1,n\text{-}1} = D_{n\text{-}1}. \quad (11)$$

Where, β is the generalized dependent variable representing u and θ for the conservation of momentum and energy respectively. While A, B, C and D are the source terms taken as depicted in [15].

3.4. Boundary conditions

At the inlet, the air velocity profile is assumed to be uniform. At outlet, the gradient of flow variables in the flow direction is set to zero. Along the axis of symmetry, the following boundary conditions were used:

$$Y = 0 \; ; \; \psi^* = 0; \frac{\partial u}{\partial \psi^*} = 0; \frac{\partial \theta}{\partial \psi^*} = 0$$

And the wall boundary conditions are:

$Y = f(X)$ (know wall geometry);

$$\psi^* = \text{constant}; \qquad U = 0; \; \frac{\partial \theta}{\partial \psi^*} = 0 .$$

3.5. Solution procedure and convergence

The system of eqs. (11) has been solved using an implicit finite difference scheme based on the arrangement shown in fig. 1. The solution procedure and convergence are realized by the algorithm depicted in [15].

3.6. Model validation

A test for the present model is carried out for a typical case of air-air ejector. So the model has been tested and validated against the published experimental and analytical results of [3]. These comparisons are presented in figs. 4 and 5 under the same conditions of primary stagnation pressure and temperature, P_{o1} and $T_{o1,}$ for the tested ejector. It is evident from fig. 4 that the present predicted wall static pressure distributions and experimental one [3] are in closer agreement compared with analytical results of [3]. While fig. 5, shows the present predicted, experimental and theoretical temperature profiles at four axial locations of [3]. The comparison shows acceptable agreement. The discrepancy of results may be due to the empirical input values of the velocity and temperature profiles at each flow section into the analytical model presented in [3] while the present model depends only on the assumed initial conditions.

For more validation of the present model, the model has been compared with the present experimental results as shown in fig. 6, for wall static pressure coefficient distributions at five different values of motive stagnation pressure coefficient. The comparison shows a reasonable agreement.

4. Optimum ejector design

The objective of optimum ejector design is to achieve a maximum efficiency through the following procedures:
1. A random value of an area ratio is chosen.
2. Operational parameters μ, λ and C_{p_o} in order to avoid shocks, separation and secondary flow recirculation are selected.
3. Minimum optimum dimensionless ejector lengths (L_a/D_b, L_b/D_b and L_c/D_b) are selected in order to minimize the overall ejector weight and to maximize the overall ejector efficiency.
4. For each optimum ejector design there are certain values of the operational parameters

which give the maximum efficiency. The optimum dimensionless lengths are correlated as functions of the ejector area ratio and the operating parameters. Both the optimum ejector lengths together with the optimum operational parameters are interpreted in optimum characteristic curves.

4.1. Optimum constant-pressure mixing section length, (L_a/D_b)

Mixing of supersonic primary flow with the subsonic secondary flow leads to an abrupt pressure rise, which leads to possible regions of recirculation or separation which are undesirable in optimum designs. A convergent section results in a higher velocity of the secondary flow (leading to its acceleration) which is accompanied by a decrease in the static pressure that equalizes, to some extent, the abrupt pressure rise due to mixing leading to an overall constant-pressure mixing. After several trials, the optimum-constant pressure mixing length is found to be the length at the end of which the flow becomes no longer supersonic.

4.2. Optimum constant-area mixing section length, (L_b/D_b)

After selection of the optimum constant-pressure mixing section length, both streams of flow are allowed to mix completely in a constant-area mixing section. The optimum length of the constant-area mixing section is the length at the end of which fully developed flow is accomplished.

4.3. Optimum diffuser section length, (L_c/D_b)

The optimum length of diffuser section is selected to recover the pressure until a certain back pressure. In all calculations in the present study, an atmospheric back pressure is chosen.
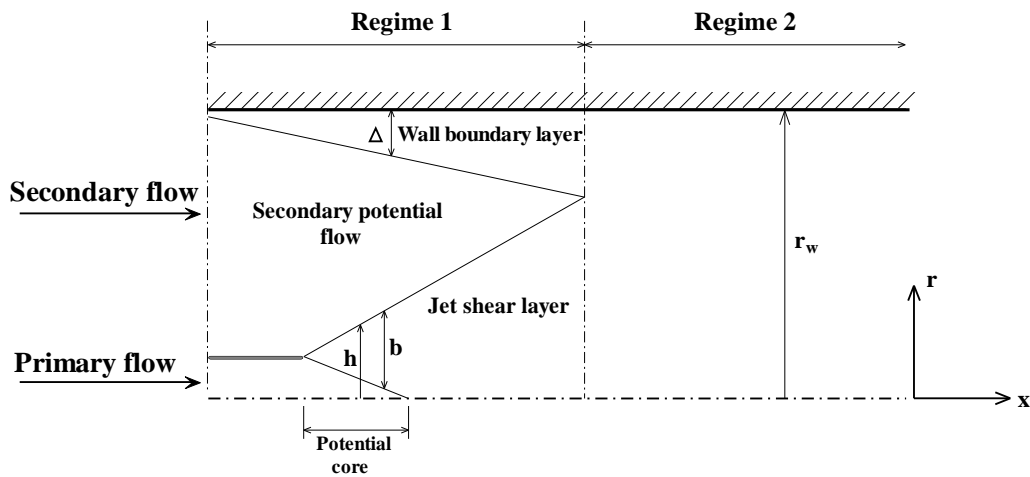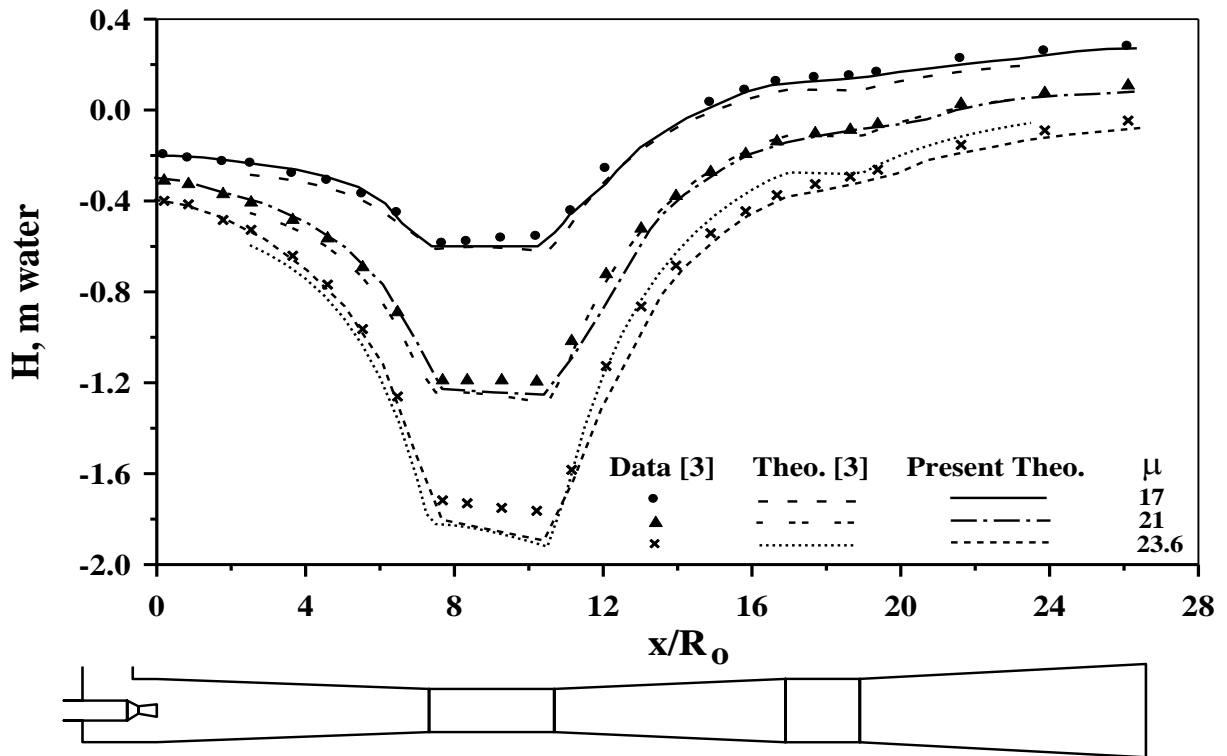
Fig. 3. Flow regions.

Fig. 4. Comparison between predicted wall static pressure distributions and published theoretical and experimental data, ref. [3] for different entrainment ratios. (P_{o1} = 24 bar , T_{o1} = 706 K).
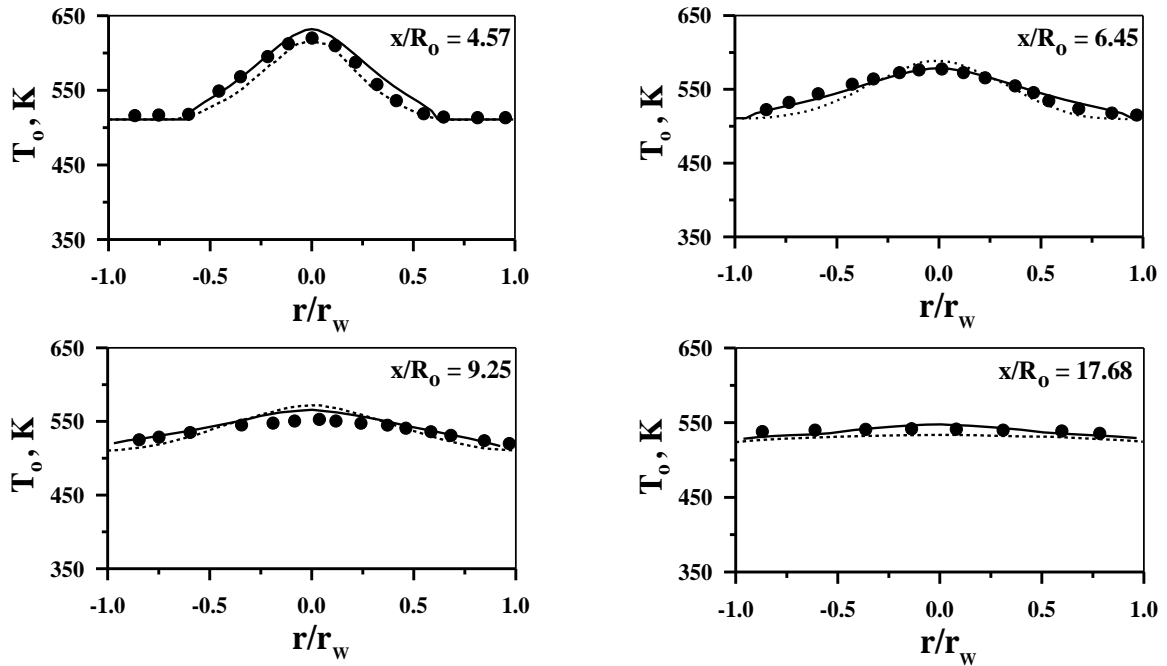
Fig. 5. Comparison between predicted radial variation of stagnation temperature and published theoretical and experimental data, ref. [3] at four axial locations. (P_{01} = 24 bar , T_{01} = 706 K).
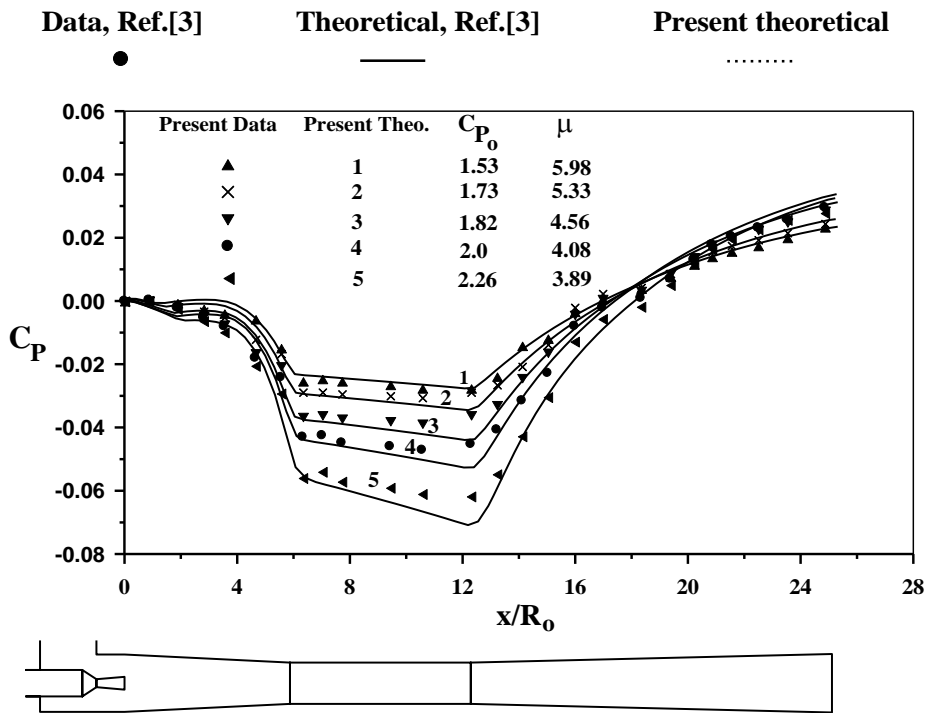

Fig. 6. Comparison between predicted wall static pressure coefficient distributions and experimental data at different inflow conditions (λ= 1.0, Ar = 17.38).
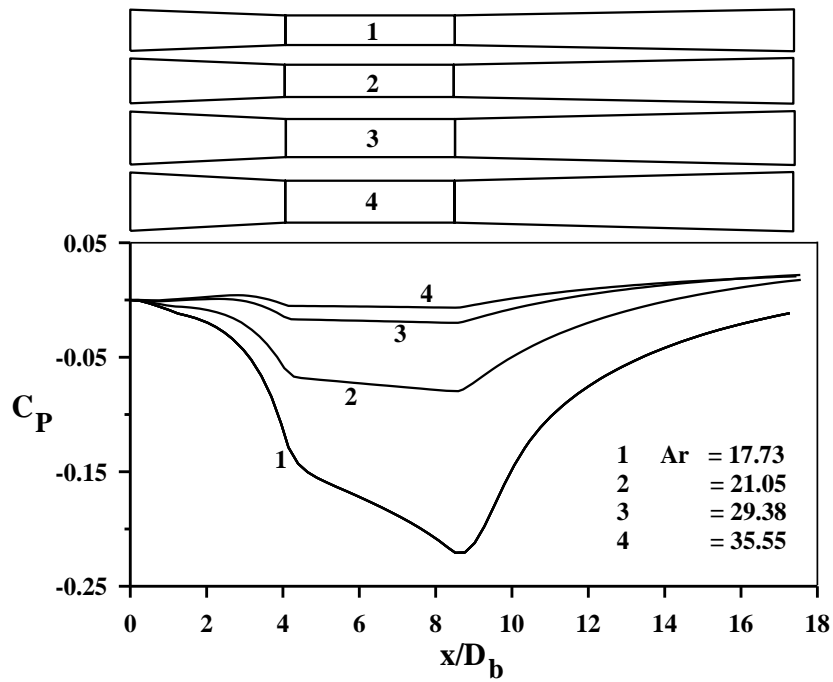
Fig. 7. Effect of area ratio on static pressure coefficient distributions along the ejector geometry,($\mu = 6$, $C_{p_o} = 1.76$, $\lambda = 1$).
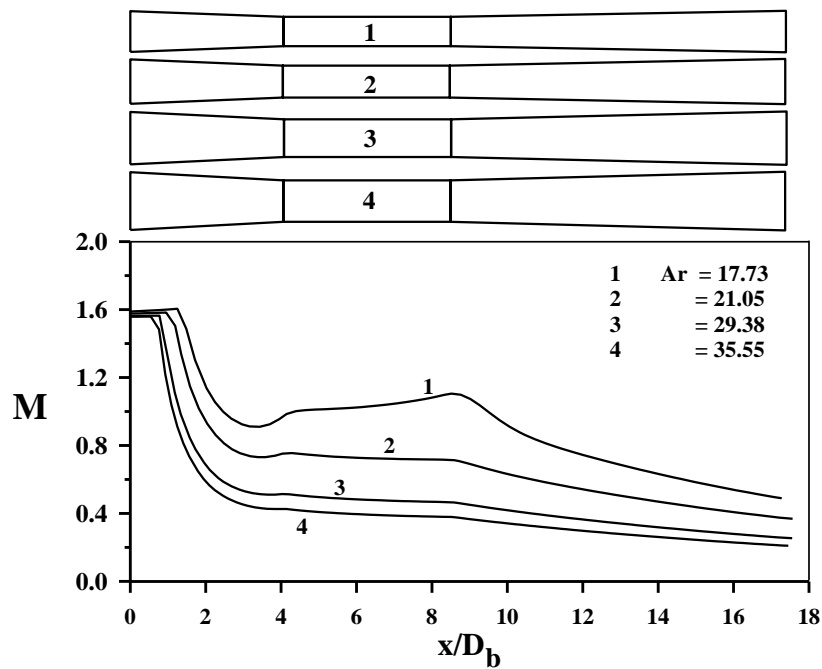

Fig. 8. Effect of area ratio on centerline Mach number distributions along the ejector geometry, ($\mu = 6$, $C_{p_o} = 1.76$, $\lambda = 1$).

5. Results and discussion

5.1. Effect of area ratio, Ar

Ejector area ratio is considered as the main geometric parameter in designing an ejector for a particular operation. The ejector area ratio (*Ar*), is defined as the ratio between the area of the constant-area mixing section and the exit area of the primary flow nozzle. The inner exit primary flow diameter is kept constant at 6.2 mm while the constant-area mixing section is varied in order to investigate the effect of (*Ar*) on ejector performance. Increasing the area ratio increases the secondary flow inlet area (where θ_1 and θ_2 are constants). A larger secondary flow area results in a smaller velocity, smaller Mach number and consequently a larger static pressure. The effect of area ratio on the static pressure coefficient and centerline flow Mach number at four different area ratios is shown in figs. 7 and 8. From these figures it is clear that *Ar*, has a positive effect on the static pressure coefficient and a negative effect on the centerline Mach number. The effect of area ratio on the ejector efficiency (η), and the pressure ratio (ϕ), at different operating conditions is shown in fig. 9.

Fig. 9-a shows the effect of area ratio on the ejector efficiency and pressure ratio at four different mass ratios. At a certain value of area ratio ejector efficiency is increased as the mass ratio increases while for a given mass ratio, ejector efficiency is increased firstly due to the increase in the area ratio which increases the static temperature of the secondary flow. However, the ejector efficiency is then decreased due to the increase in total energy loss represented in the exit stagnation pressure, P_{oe}. Fig. 9-b shows the effect of area ratio on the ejector efficiency and pressure ratio at six different temperature ratios. For a given value of area ratio, efficiency is increased as the temperature ratio decreases because of a decrease in the primary flow static temperature. While for a given value of temperature ratio, the ejector efficiency is firstly increased due to an increase in the static temperature of the secondary flow but it is then decreased due to the increase in the frictional losses associated with decreasing the

exit stagnation pressure, *Poe*. Fig. 9-c represents the effect of area ratio on the ejector efficiency and pressure ratio at four different stagnation pressure coefficients. At a certain area ratio, a lower stagnation pressure coefficient leads to efficiency enhancement due to power saving represented in a lower primary flow stagnation pressure. While at a certain value of C_{p_o}, efficiency is firstly increased due to an increase in the secondary flow static temperature, T_2 and it is then decreased due to a decrease in exit stagnation pressure at ejector exit.

5.2. Optimum characteristic curves

To obtain the optimum characteristic curves through the previously mentioned optimization procedures, five values of area ratios *Ar*, are selected 9.78, 17.38, 39.11, 108.65 and 278.14. For each area ratio, the operational parameters λ, μ and C_{p_o} are chosen by systematic trial together with the optimum ejector dimensionless lengths L_a/D_b, L_b/D_b and L_c/D_b.

The five previously mentioned area ratios are separately investigated to develop correlations relating ejector maximum efficiency, pressure ratio and ejector optimum dimensionless lengths with area ratio and operational parameters. The area ratio under investigation is kept constant and the operational parameters λ, μ and C_{p_o} are varied systematically one by one while keeping the others as constants. The maximum efficiency is selected with its pressure ratio and the ejector optimum dimensionless lengths and so on. The obtained results are used in developing new CFD based formulas relating all the parameters under study. The obtained correlations for air-driven air ejectors with $\theta_1=5.4°$ and $\theta_2=2.7°$, are in the following forms;

$$\frac{L_a}{D_b} = \frac{6.605 \, C_{P_o}^{\,2.193} \, \mu^{0.595}}{\lambda^{0.507} \, Ar^{1.115}} \qquad . \tag{12}$$
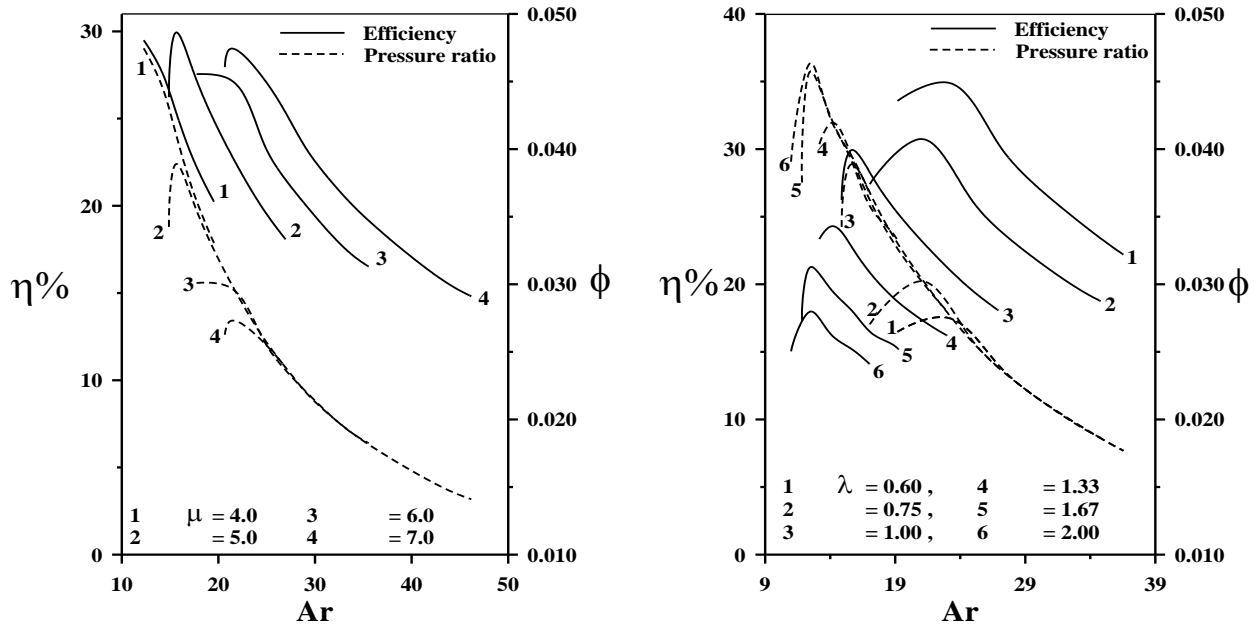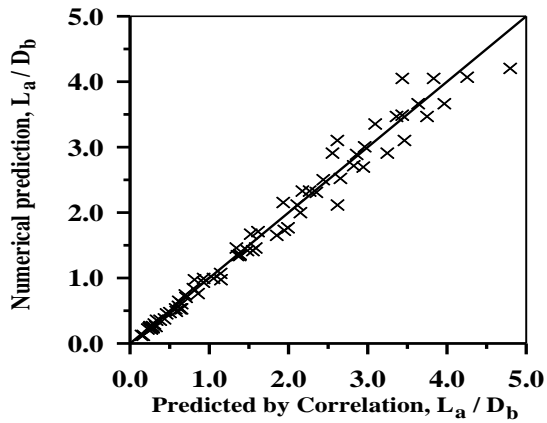
a- Effect of mass ratio, (C_{p_o} = 1.76, λ = 1.0).

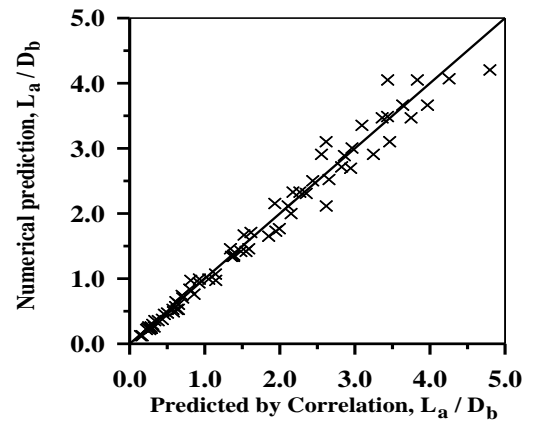b- Effect of temperature ratio, (C_{p_o} = 1.76, μ = 5).
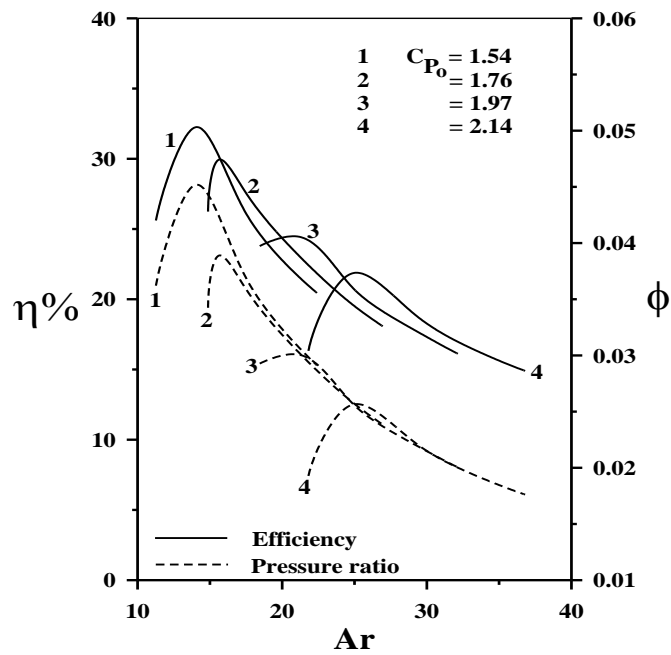
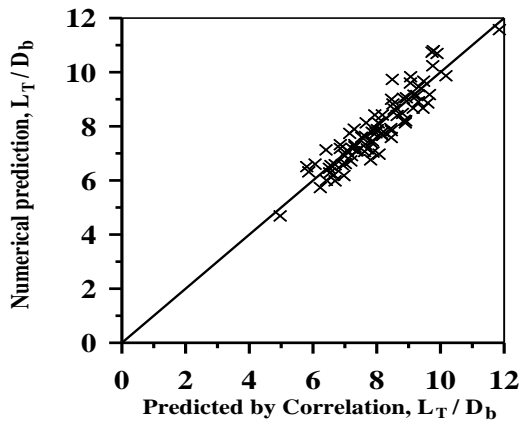c- Effect of stagnation pressure coefficient, (μ = 5, λ = 1.0).

Fig. 9. Effect of area ratio on ejector efficiency and pressure ratio for different inflow conditions.
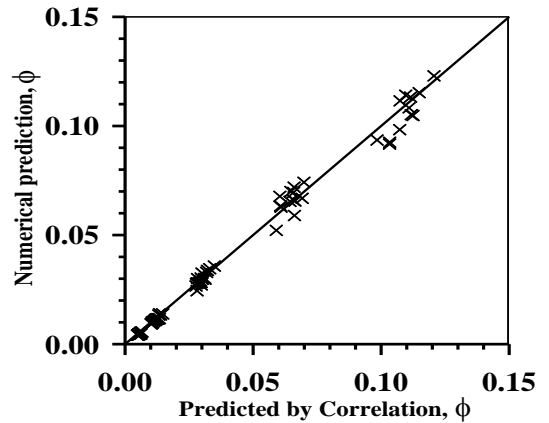
a- $\dfrac{L_a}{D_b} = \dfrac{6.605 \; C_{P_o}^{\;2.193} \; \mu^{0.595}}{\lambda^{0.507} \; Ar^{1.115}}$

b- $\dfrac{L_a + L_c}{D_b} = \dfrac{8.787 \; C_{P_o}^{\;2.071} \; \mu^{1.509}}{\lambda^{0.693} \; Ar^{1.303}}$

c- $\dfrac{L_T}{D_b} = \dfrac{8.545 \; C_{P_o}^{\;0.827} \; \mu^{0.837}}{\lambda^{0.496} \; Ar^{0.572}}$

d- $\phi = \dfrac{1.048 \; \lambda^{0.13}}{C_{P_o}^{\;0.498} \; \mu^{0.393} Ar^{0.662}}$
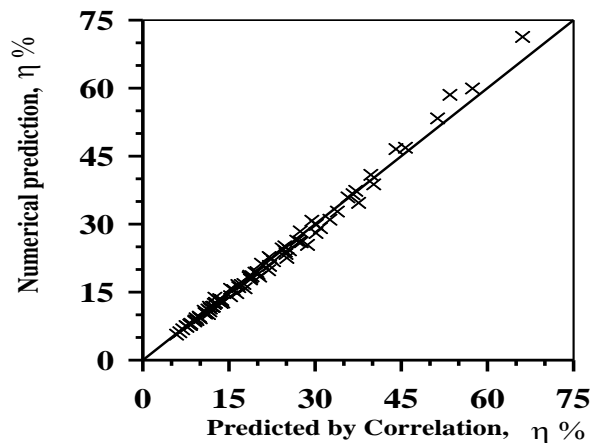
e- $\eta = \dfrac{132.81 \; \mu^{0.439}}{C_{P_o}^{\;0.0938} \; \lambda^{0.77} \; Ar^{0.587}}$

Fig. 10. Comparison between numerical prediction and values predicted by correlations (10-14).

Fig. 11. Optimum characteristic curves for ejector performance at five different area ratios.

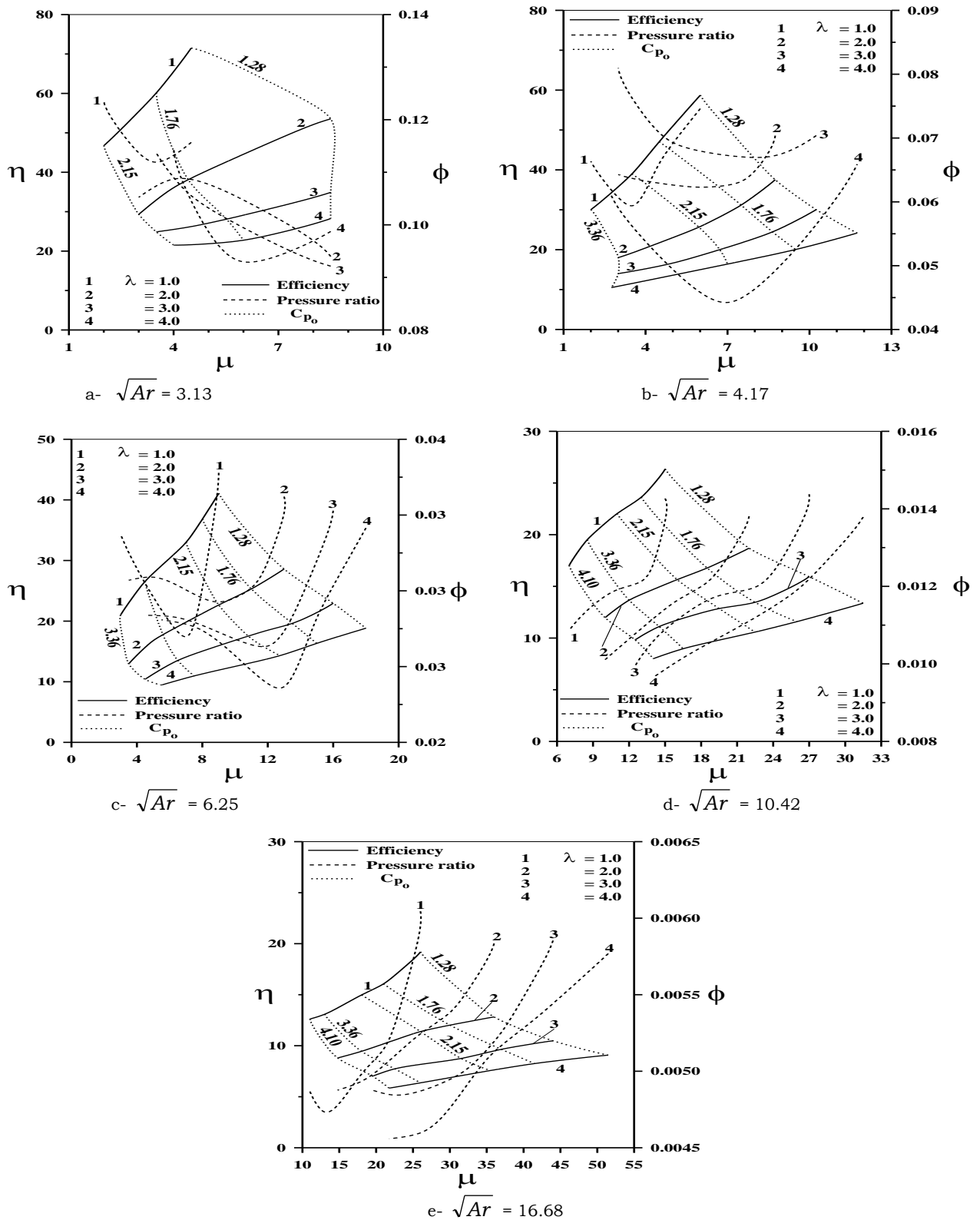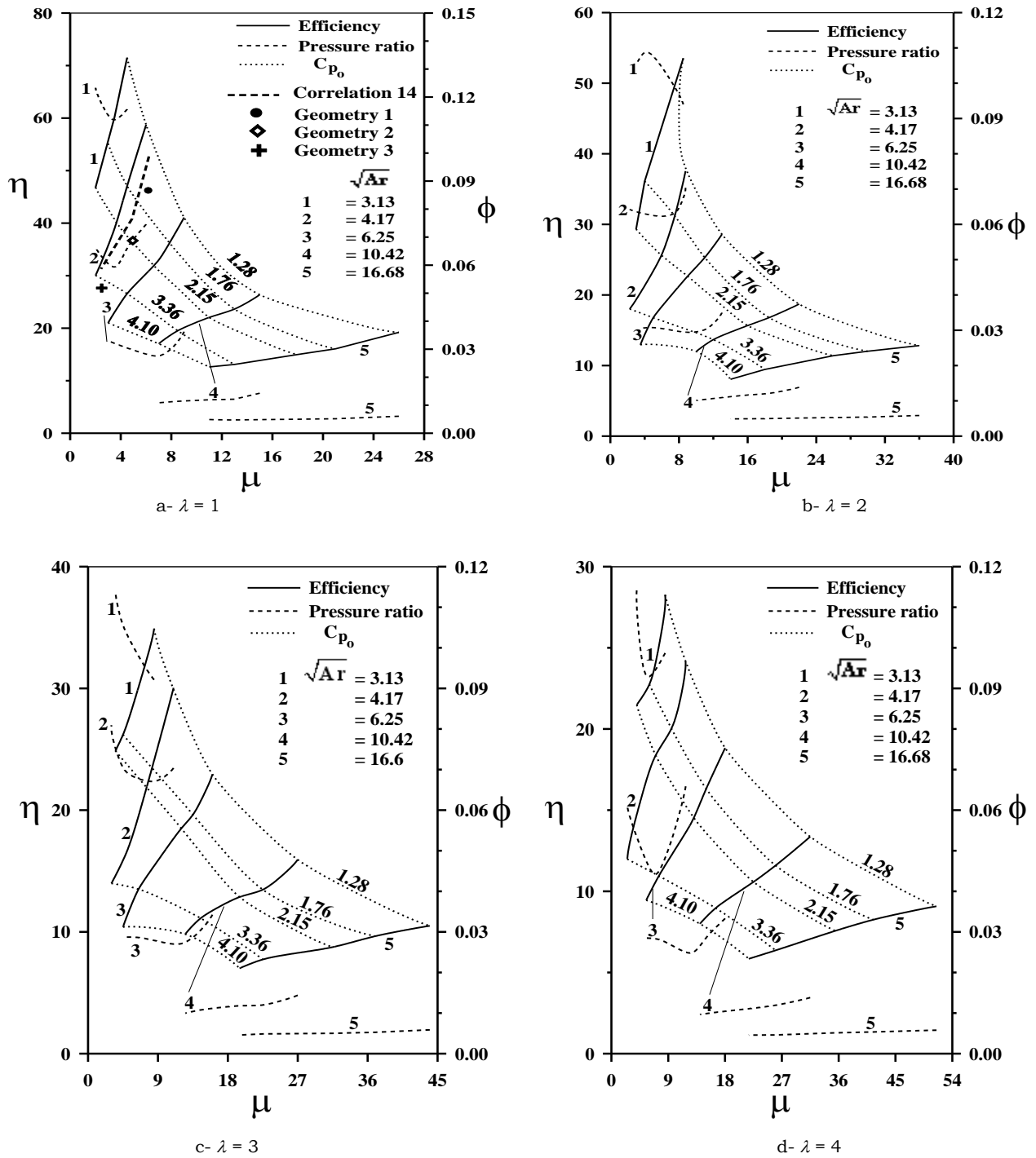Fig. 12. Optimum characteristic curves for ejector performance at four different temperature ratios.

$$\frac{L_a + L_c}{D_b} = \frac{8.787 \, C_{P_o}^{2.071} \, \mu^{1.509}}{\lambda^{0.693} \, Ar^{1.303}} \quad . \tag{13}$$

$$\frac{L_T}{D_b} = \frac{8.545 \, C_{P_o}^{0.827} \, \mu^{0.837}}{\lambda^{0.496} \, Ar^{0.572}} \quad . \tag{14}$$

$$\phi = \frac{1.048 \, \lambda^{0.13}}{C_{P_o}^{0.498} \, \mu 0.393 \, Ar^{0.662}} \, , \tag{15}$$

$$\eta = \frac{132.81 \, \mu^{0.439}}{C_{P_o}^{0.0938} \, \lambda^{0.77} \, Ar^{0.587}} \quad . \tag{16}$$

A comparison between the numerical results and the values obtained by the deduced formulas is represented in fig. 10. The formulas are validated for an area ratio of $(9.78 \le Ar \le 278.14)$, a mass ratio of $(2 \le \mu \le 51)$, a temperature ratio of $(1 \le \lambda \le 4)$ and with a stagnation pressure coefficient of $(1.28 \le C_{P_o} \le 4.10)$.

Fig. 11 illustrates the optimum characteristic curves for ejector selection under maximum efficiency at five different area ratios. Intermediate values of temperature ratios can be obtained by interpolation.

Fig. 12 represents the optimum characteristic curves of a certain ejector at four different temperature ratios in order to operate at a maximum efficiency. The formulas obtained are then used to determine the optimum lengths of the ejector. For example, from fig. 12-a if it is required to operate with a mass ratio of $\mu = 8$ for an isothermal ejector $(\lambda = 1)$ then the optimum stagnation pressure coefficient should be 1.28 which gives an optimum efficiency of 36% and a pressure ration of 0.03 at an area ratio of 39.11. However, the efficiency and pressure ratio would be about 46.5% and 0.045 respectively if a square root of an area ratio is chosen by interpolation to be about 5.6, $(Ar = 31.36)$. Then the optimum ejector dimensionless lengths could be obtained from the formulas eq. (12 to 14) for a particular values of μ, λ, Ar and C_{P_o}. To validate the performed optimization, three optimized geometries, the dimensions of which can be obtained from

correlations eq. (12 to 14) with an area ratio of 17.38, are selected from the optimum design charts and the correlations, fabricated and experimentally tested. The obtained results are compared with that theoretically predicted and also with that obtained from the correlations. The comparison shown in fig. 12-a shows a reasonable agreement.

6. Conclusions

The present study is concerned with numerical and experimental investigation of supersonic primary flow and subsonic secondary flow air-air ejectors. The present theoretical and experimental results are well compared with the published data. Formulas for ejector optimum (maximum efficiency) design are obtained by fitting the numerical results and relating the ejector operation parameters to the ejector optimum geometric dimensionless parameters, pressure ratio and optimum efficiency.

Nomenclature

A_{n-1} is the coefficient in the finite-difference eq. (9),

Ar is the area ratio, s,

b is the local jet shear layer width,

B_{n-1} is the coefficient in the finite-difference eq. (9),

$\bar{c}_p$ is the time-average specific heat at constant pressure,

$c_p{}^*$ is the dimensionless specific heat, $\dfrac{\bar{c}_p}{c_{p1}}$,

c_{p1} is the specific heat at nozzle exit plane,

C_L is the eckert number, $\dfrac{(\gamma - 1) \, M_1^2}{\dfrac{T_{wr}}{T_1} - 1}$,

C_{n-1} is the coefficient in the finite-difference eq. (9),

C_p is the wall static pressure coefficient, $\dfrac{P_i - P_1}{0.5 \, \rho_1 \, u_1^2}$

C_{P_o} is the primary flow stagnation pressure coefficient, $\dfrac{P_{o1} - P_{ref}}{0.5 \, \rho_1 \, U_1^2}$,

d is the internal exit diameter of the primary flow nozzle,

D is the diameter of the constant pressure mixing section at the nozzle exit plane,

D_b is the diameter of the constant area mixing section,

D_{n-1} is the coefficient in the finite-difference eq. (9),

E is the dimensionless eddy viscosity, $\dfrac{\varepsilon}{\nu_1}$,

H is the wall static pressure head,

h is the distance from shear layer outer edge to the jet centerline,

$\bar{k}$ is the time-average thermal conductivity,

k_1 is the thermal conductivity of primary flow at nozzle exit plane,

l_m is the mixing length,

L_m is the dimensionless mixing length,

L_a is the constant-pressure mixing section length,

L_b is the constant-area mixing section length,

L_c is the diffuser section length,

L_T is the total length of the diffuser $(L_a + L_c + L_c)$,

m^o is the mass flow rate,

M is the mach number,

M_1 is the primary flow mach number at nozzle exit plane, $\dfrac{U_1}{(\gamma R T_1)^{1/2}}$,

$\bar{p}$ is the time-average static pressure,

p is the dimensionless pressure $\dfrac{\bar{p}}{0.5 \rho_1 U_1^2}$,

P is the wall static pressure,

P_o is the stagnation pressure,

P_{ref} is the reference atmospheric pressure,

P_{rt} is the turbulent Prandtl number, $\dfrac{\varepsilon}{\varepsilon_H}$,

P_{r1} is the prandtl number, $\dfrac{\mu_1 c_{p1}}{k_1}$,

Q is the dimensionless parameter in eq. (7),

q_T is the turbulent heat transfer, $\overline{(\rho v)' T'}$,

S is the dimensionless parameter in eqs. (6 and 7),

T is the local static temperature,

$\bar{T}$ is the time-average temperature,

T' is the instantaneous fluctuating temperature,

T_o is the stagnation temperature,

T_{wr} is the wall reference temperature,

$\bar{u}$ is the time-average velocity in x-direction,

u' is the instantaneous fluctuating axial velocity component,

U is the local axial velocity in x-direction

u is the dimensionless velocity in x-direction, $\dfrac{\bar{u}}{U_1}$,

$\bar{v}$ is the time-average flow velocity in r-direction,

v' is the instantaneous fluctuating radial velocity component,

x is the space coordinate in the axial direction,

X is the dimensionless space coordinate, $\dfrac{U_1 x}{\nu_1}$,

ΔX is the step size in x-direction,

r is the space coordinate in the radial direction,

Y is the dimensionless space coordinate in the radial direction, $\dfrac{U_1 r}{\nu_1}$,

V is the volume flow rate,

η is the ejector efficiency $= \dfrac{V_2}{V_1} \dfrac{(P_{oe} - P_{o2})}{(P_{o1} - P_{oe})} = \mu \dfrac{T_2}{T_1} \dfrac{\phi}{(1-\phi)}$,

ϕ is the pressure ratio, $\dfrac{P_{oe} - P_{o2}}{P_{o1} - P_{o2}}$,

λ is the stagnation temperature ratio, $\dfrac{T_{o1}}{T_{o2}}$,

ψ is the stream function,

ψ^* is the dimensionless stream function,

$$\psi^{*2} = \frac{\psi^2 u_1}{\rho_1 \upsilon_1^2} \quad \text{(for axisymmetric flow),}$$

ρ is the fluid density,

$\overline{\rho}$ is the time-average fluid density,

ρ^* is the dimensionless fluid density, $\dfrac{\overline{\rho}}{\rho_1}$,

μ is the mass ratio, $\dfrac{m^o_2}{m^o_1}$,

$\overline{u}$ is the time-average absolute viscosity,

μ^* is the dimensionless absolute viscosity, $\dfrac{\overline{\mu}}{\mu_1}$,

μ_1 is the primary flow viscosity at nozzle exit plane,

τ is the local shear stress,

τ_T is the turbulent shear stress, $\overline{(\rho\upsilon)' \, u'}$,

ε is the eddy momentum diffusivity,

ε_H is the eddy thermal diffusivity,

θ is the dimensionless temperature, $\dfrac{\overline{T} - T_1}{T_{wr} - T_1}$,

θ_1 is the total angle of constant pressure mixing section,

θ_2 is the total angle of diffuser section,

υ is the kinematic viscosity,

δ is the local wall boundary layer thickness, and

Δ is the dimensional boundary layer thickness, $\dfrac{u_1 \delta}{\upsilon_1}$.

Subscripts

1   is the primary stream condition at nozzle exit plane,

2   is the secondary stream condition at nozzle exit plane,

e is the mixing section exit condition,

i is the an integer number denoting the pressure tap number or location of pressure, and

w is the wall condition.

References

[1] P.H. Donald and W.C. Robert, "Investigation at Supersonic and Subsonic Mach Numbers of Auxiliary Inlets Supplying Secondary Air Flow to Ejector Exhaust Nozzles", NACA RM E55J12a, January 25 (1956).

[2] J. Fabri and J. Paulon, "Theory and Experiments on Supersonic Air-to-Air Ejectors", NACA TM-1410, September (1958).

[3] N.G. Kirti, T.P. Torda and L. Zalman, "Turbulent Mixing in the Initial Region of Heterogeneous Axisymmetric Coaxial Confined Jets", NASA CR-1615, May (1970).

[4] F.A. Abou-Taleb, "Effect of Geometric Parameters on the Performance of Ejectors", M. Sc. Thesis, Department of Mechanical Engineering, Menoufia University, Egypt (1986).

[5] J.C. Dutton and B.F. Carroll, "Optimal Supersonic Ejector Design", Trans. ASME, Vol. 108, pp. 414-420 (1986).

[6] G. Raman and R. Taghavi "Aeroacoustic Characteristics of a Rectangular Multi-Element Supersonic Jet Mixer-Ejector Nozzle", Int. J. Sound and Vibration, Vol. 207 (2), pp. 227-247 (1997).

[7] D.W. Guillaume and T.A. Judge, "Improving the Efficiency of a Jet Pump Using an Elliptical Nozzle", Review of Scientific Instrument, Vol. 70 (12), pp. 4727-4729 (1999).

[8] S. Szabo, "Influence of the Material Quality of Primary Gas Jets on the Final Vacuum Created by a Supersonic Gas Ejector", J. Computational and Applied Mechanics, Vol. 2 (1), pp. 131-144 (2001).

[9] M.T. Kandakure V.G. Gaikar and A.W. Patwardhan, "Hydrodynamic Aspects of Ejectors", Chemical Engineering Science, Vol. 60, pp. 6391-6402 (2005).

[10] S.N. Karambirov and V.F. Chebaevskii "Possibilities of Improving Ejector Pump Characteristics", Chemical and Petroleum Engineering, Vol. 41 (1-2), pp. 75-80 (2005).

[11] F. Yong, S. Yuji and K. Nobuhide, "Development of a Large-Entrainment-

Ratio Axisymmetric Supersonic Ejector for Micro Butane Combustor", J. Micromech. Microeng., Vol. 16, pp. S211-S219 (2006).

[12] E. Krause, "Numerical Treatment of Boundary-Layer and Navier-Stokes Equations", VKI Lecture Series, "Numerical Methods in Fluid Mechanics" pp. 7-11 (1972).

[13] K.R. Hedges and P.G. Hill, "Compressible flow Ejectors", J. Fluid Engineering, Trans. ASME, Vol. 96, pp. 272-281 (1974).

[14] H. Schlichting, "Boundary Layer Theory", McGraw-Hill Book, Inc., New York (1968).

[15] N.I. Hewedy M.H. Hamed, F. Abou-Taleb Sh. and T.A. Ghonim, "Numerical and Experimental Investigation of Compressible Flow Ejectors", Minoufiya Engineering Research Journal, Vol. 30 (1), pp. 53-66 (2007).